

## Supporting Material

### Mapping the processivity determinants of the kinesin-3 motor domain

Guido Scarabelli,<sup>1</sup> Virupakshi Soppina,<sup>2</sup> Xin-Qiu Yao,<sup>1</sup> Joseph Atherton,<sup>3</sup> Carolyn A. Moores,<sup>3</sup>  
Kristen Verhey,<sup>2,\*</sup> and Barry J. Grant<sup>1,\*</sup>

<sup>1</sup>Department of Computational Medicine and Bioinformatics, and <sup>2</sup>Department of Cell and Developmental Biology, University of Michigan Medical School, MI, USA. <sup>3</sup>Institute of Structural and Molecular Biology, Birkbeck College, University of London, UK

\*Correspondence to K.V. [kjverhey@umich.edu](mailto:kjverhey@umich.edu) and B. J. G. [bjgrant@umich.edu](mailto:bjgrant@umich.edu)

## Materials and methods

### *Molecular dynamics simulations*

Simulation models were based on the crystallographic structures of human kinesin-1 in complex with the microtubule in the ATP and Apo states (PDB codes 4HNA and 4LNU) (1) (2) and on the CryoEM structures for human kinesin-3 in ATP, Apo and ADP states (PDB codes 4UXP, 4UXO, 4XUS) (3). The kinesin-1 ADP state complex was built from initially merging a kinesin-1 ADP state structure (PDB code 1BG2) with tubulin from a kinesin-3 ADP complex structure (PDB code 4XUS) via superposition based on the  $\alpha 4$  helix (residues 255-270 in kinesin-1 and 278-293 in kinesin-3). A loop refinement optimization was performed on the kinesin-1 ADP state complex with Modeller v9.10 (4) for L8c segment (residues 158-162), L11 (residues 237-253), L12 (residues 271-276) and the neck-linker (residues 326-337) and evaluated using the discrete optimized protein energy score (5). All kinesin-tubulin model structures were built with the AMBER 12 package (6) and corresponding all-atom potential function ff99SB (7). Models were inserted in a cubic water box with margins located 12Å from the closest protein atom. The energetic parameters for the nucleotide molecules were obtained from the AMBER parameter database (8). TIP3P water molecules and sodium counter ions were added to each system. Four runs of energy minimization of 4000 cycles each were employed alternating every 100 cycle the steepest descent and the conjugate gradient algorithms. Positional restrains with a force of 500 kcal / (mol Å<sup>2</sup>) were applied in the first run on all protein and ligand atoms. In the second run the restrains were applied on the protein backbone only and in the third run on the water and counter ions only. In the fourth run no atoms were restrained. A fifth energy minimization run of 4000 cycles was then performed using the conjugate gradient algorithm only and no atomic restrains. Two subsequent molecular dynamics runs of 10ps and 200ps were employed to increase each system temperature from 100K to 300K and to equilibrate each system configuration at 300K. The production runs started from these equilibrated conformations. Periodic boundary conditions and full particle-mesh Ewald electrostatics were used. A 12Å cutoff value was included for truncation of non-bonded interactions. The simulations were run at constant temperature (300 K) and constant pressure (1 atm) with a 2fs time step. The SHAKE algorithm was used to constrain all covalent bonds involving hydrogen atoms. Each simulation was 40ns long, and was reproduced four times with random initial velocity assignments, for a total of 160ns of production phase dynamics for each system.

### *MM/GBSA calculations*

Molecular mechanics with generalized Born and surface area solvation (MM/GBSA) binding energy calculations were performed with the GB<sup>OBC</sup> model (9) in AMBER 12 (6). For each simulated system, pairwise energy values (resulting from setting idecomp=4) were scaled by the average number of kinesin-microtubule interaction pairs in both in kinesin-1 and kinesin-3 (39 average contacts) and averaged over four replicate simulations. The total binding free energies reported in the main text were scaled by a factor of 0.3. This was obtained from linear fitting to experimental microtubule dissociation constants determined by Hirokawa and coworkers for kinesin-3 (10). Results obtained from the combined analysis of structural interactions across models of all nucleotide states of each kinesin were used to inform experiential site-directed mutagenesis studies. Residue level comparisons of kinesin-1 and kinesin-3 motor domains utilized a Bio3D structure based sequence alignment that mapped all equivalent (aligned) and non-equivalent (un-aligned) regions (11).

### *Site-directed mutagenesis*

Mutations were introduced into plasmids encoding constitutively motile, dimeric versions of kinesin-3 KIF1A(1-393)LZ-3xmCitrine (12). All mutations were introduced using QuikChange site-directed mutagenesis (Agilent Technologies) and verified by DNA sequencing of both strands.

### *Cell Culture, Transfection and Cell Lysates*

COS-7 (monkey kidney fibroblast, ATCC) cells were grown in DMEM + 10% (vol/vol) FBS and 2 mM L-glutamine at 37 °C with 5% (vol/vol) CO<sub>2</sub>. Cells were transfected with 1.0 µg of plasmid DNA using Expressfect (Danville Scientific). After 16 hrs of transfection, the cell lysates were prepared as described previously (12). Briefly, COS-7 cells expressing fluorescent protein-tagged motors were trypsinized and pelleted by low-speed centrifugation at 4 °C. The pellet was washed once with cold DMEM culture medium and lysed in ice-cold lysis buffer (25 mM HEPES/KOH, 115 mM potassium acetate, 5 mM sodium acetate, 5 mM MgCl<sub>2</sub>, 0.5 mM EGTA, and 1% Triton X-100, pH 7.4) freshly supplemented with 1 mM PMSF and protease inhibitors (10 µg/mL leupeptin, 5 µg/mL chymostatin, 3 µg/mL elastatinal, and 1 mg/mL pepstatin). The lysate was clarified by centrifugation at 16,000 × g at 4 °C and either used fresh for assays or aliquots were frozen in liquid nitrogen and stored at -80 °C until further use.

### *Microtubule polymerization*

Microtubules were polymerized from purified tubulin (TL238, Cytoskeleton) in BRB80 buffer (80 mM Pipes/KOH pH 6.8, 1 mM MgCl<sub>2</sub>, 1 mM EGTA) supplemented with 1mM GTP at 37 °C for 20 min, stabilized by addition of 5 volumes of pre-warmed BRB80 containing 20 μM taxol, incubated for 5 min, and then stored at room temperature.

### *Total Internal Reflection Fluorescence Single-Molecule Motility Assays*

All single-molecule assays were performed at room temperature using a Nikon Ti-E objective-type total internal reflection fluorescence (TIRF) microscope with Perfect Focus System, a 100× 1.49 N.A. CFI APO TIRF objective, an Agilent 3-Line (488, 561, and 640 nm) Monolithic Standard Power Laser Launch with AOTF, an EMCCD camera (iXon+ DU897; Andor), and controlled by Nikon Elements image acquisition software. A narrow motility chamber (~10 μl volume) was assembled by attaching a clean #1.5 coverslip to a microscope slide with double-sided tape. Polymerized microtubules were diluted in P12 buffer (12 mM Pipes/KOH pH 6.8, 1 mM MgCl<sub>2</sub>, 1 mM EGTA) containing 10 μM taxol and then introduced into the motility chamber and incubated for 5 min at room temperature to adsorb onto the coverslip. Subsequently, 50 μl of blocking buffer (10 mg/ml BSA in P12 buffer with 10 μM taxol) was introduced and incubated for 20 min to prevent non-specific binding of kinesin motors onto the coverslip surface. Finally, kinesin motors in a 50 μl Motility Mix (0.1 – 2.0 μl of COS-7 cell lysate with 30 μl of blocking buffer, 15 μl of P12 buffer, 2 mM ATP, 0.5 μl of 100 mM DTT, 0.5 μl of 100 mM MgCl<sub>2</sub>, and 0.5 μl each of 20 mg/ml glucose oxidase, 8 mg/ml catalase and 1M glucose) was added to the flow chamber and the ends were sealed with molten paraffin wax and imaged at 10 frames/sec without binning and at low laser power to avoid photobleaching during processive motor runs.

### *Data Analysis*

The position of fluorescent motor spots was manually tracked frame-by-frame using a custom-written plugin in ImageJ (nih.gov). The velocities and run lengths of individual motors were binned and histograms were generated for the population by plotting the number of events in each bin. The average velocity and run length were then obtained by fitting either a single Gaussian peak (velocity) or an exponential (run length) to the population histogram. The measurements for each construct come

from at least two independent protein preparations and include motile events lasting at least five frames (500 ms). All data are presented as mean  $\pm$  standard error of mean (SEM).

## Supporting References

1. Gigant, B., W. Wang, B. Dreier, Q. Jiang, L. Pecqueur, A. Pluckthun, C. Wang, and M. Knossow. 2013. Structure of a kinesin-tubulin complex and implications for kinesin motility. *Nature Stru Mol Bio* 20:1001-1007.
2. Cao, L., W. Wang, Q. Jiang, C. Wang, M. Knossow, and B. Gigant. 2014. The structure of apo-kinesin bound to tubulin links the nucleotide cycle to movement. *Nature Commun* 5:5364.
3. Atherton, J., I. Farabella, I. M. Yu, S. S. Rosenfeld, A. Houdusse, M. Topf, and C. A. Moores. 2014. Conserved mechanisms of microtubule-stimulated ADP release, ATP binding, and force generation in transport kinesins. *eLife* 3:e03680.
4. Sali, A., and T. L. Blundell. 1993. Comparative protein modelling by satisfaction of spatial restraints. *J Mol Biol* 234:779-815.
5. Shen, M. Y., and A. Sali. 2006. Statistical potential for assessment and prediction of protein structures. *Prot Sci* 15:2507-2524.
6. Case, D. A., T. A. Darden, T. E. I. Cheatham, T. E. Simmerling, J. Wang, R. E. Duke, R. Luo, R. C. Walker, W. Zhang, K. M. Merz, B. Roberts, S. Hayik, A. Roitberg, G. Seabra, J. Swails, A. W. Götz, I. Kolossváry, K. F. Wong, F. Paesani, J. Vanicek, R. M. Wolf, J. Liu, X. Wu, S. R. Brozell, T. Steinbrecher, H. Gohlke, Q. Cai, X. Ye, M.-J. Hsieh, G. Cui, D. R. Roe, D. H. Mathews, M. G. Seetin, R. Salomon-Ferrer, C. Sagui, V. Babin, T. Luchko, S. Gusarov, A. Kovalenko, and P. A. Kollman. 2012. AMBER 12. University of California, San Francisco.
7. Hornak, V., R. Abel, A. Okur, B. Strockbine, A. Roitberg, and C. Simmerling. 2006. Comparison of multiple Amber force fields and development of improved protein backbone parameters. *Proteins* 65:712-725.
8. Meagher, K. L., L. T. Redman, and H. A. Carlson. 2003. Development of polyphosphate parameters for use with the AMBER force field. *J Comp Chem* 24:1016-1025.
9. Onufriev, A., D. Bashford, and D. A. Case. 2004. Exploring protein native states and large-scale conformational changes with a modified generalized born model. *Proteins* 55:383-394.
10. Nitta, R., M. Kikkawa, Y. Okada, and N. Hirokawa. 2004. KIF1A alternately uses two loops to bind microtubules. *Science* 305:678-683.
11. Grant, B.J., Rodrigues, A. P. C., ElSawy, K. M., McCammon, J. A., & Caves, L. S. D. 2006. Bio3D: an R package for the comparative analysis of protein structures. *Bioinformatics* 22, 2695–2696.
12. Soppina, V., S. R. Norris, A. S. Dizaji, M. Kortus, S. Veatch, M. Peckham, and K. J. Verhey. 2014. Dimerization of mammalian kinesin-3 motors results in superprocessive motion. *Proc Nat Acad Sci U S A* 111:5562-5567.

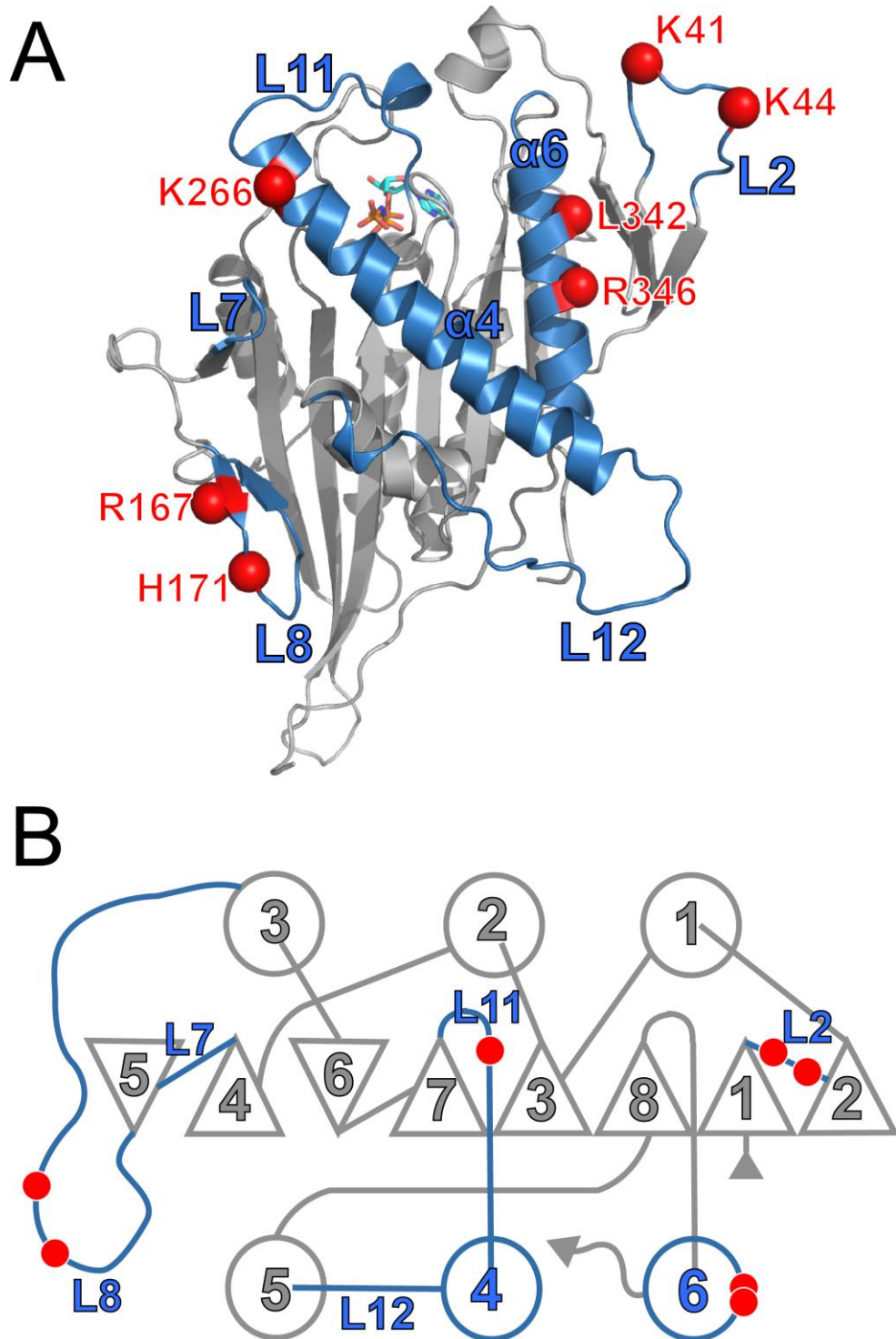


**Figure S1. Kinesin-3 motor domain structure.** (A) Kinesin regions displaying major energetic interactions with microtubule residues are rendered in blue. Red spheres indicate the location of mutation sites investigated in the current study. (B) Topological diagram of the kinesin-3 motor domain. Major  $\beta$ -strands are depicted as triangles and  $\alpha$ -helices as circles. Regions are colored as in panel A.

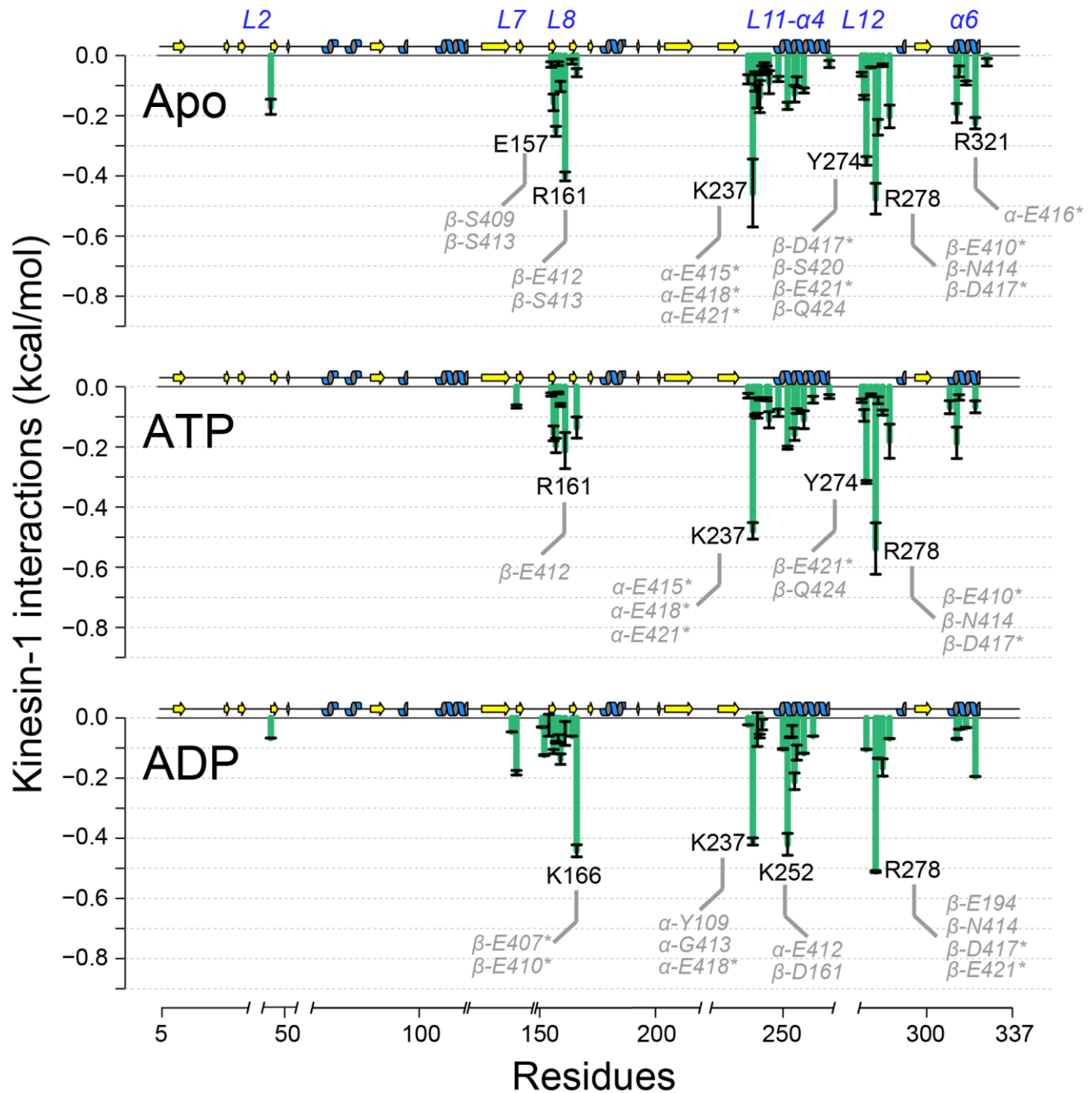


**Figure S2. Kinesin-1 residue contributions to tubulin binding energy.** Kinesin residues with prominent contributions are labeled in black and their major tubulin interacting partners are labeled in gray.

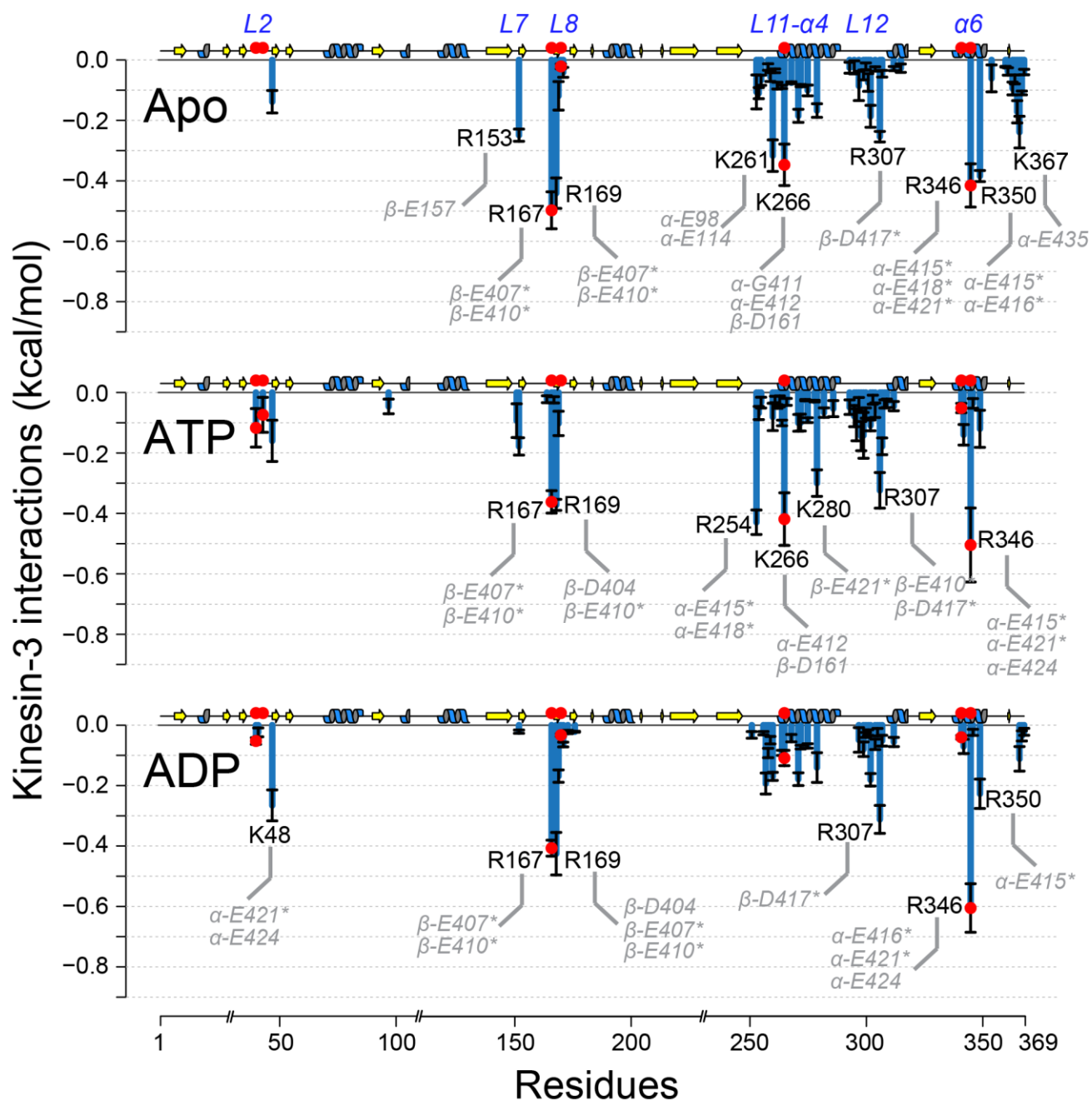


**Figure S3. Kinesin-3 residue contributions to tubulin binding energy.** Kinesin residues with prominent contributions are labeled in black and their major tubulin interacting partners are labeled in gray. The location of residues subjected to mutagenesis simulations and single molecule experiments are indicated with red points.



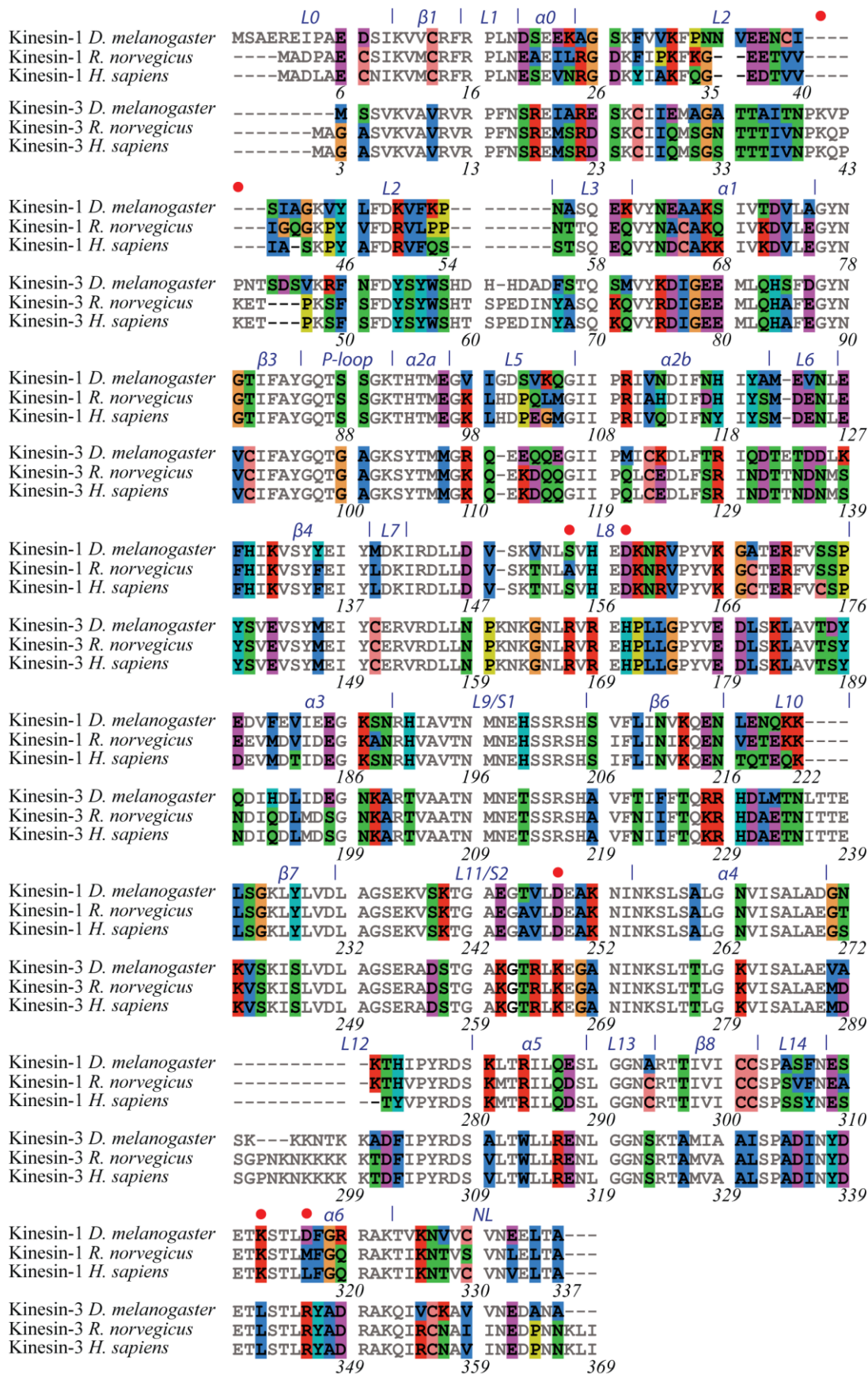


**Figure S4.** (Previous page). **Kinesin-1 and kinesin-3 structure based sequence alignment.** Residue numbers (black text) refer to Kinesin-1 and Kinesin-3 *H. sapiens*. Positions with divergent residue types are colored by their physiochemical properties (red positively charged; purple negatively charged; blue apolar; green polar; cyan Tyrosine and Histidine; Glycine orange; Cysteine pink and Proline yellow). Red dots indicate the positions of experimental mutations noted in the main text. Blue labels reference major secondary structure elements.

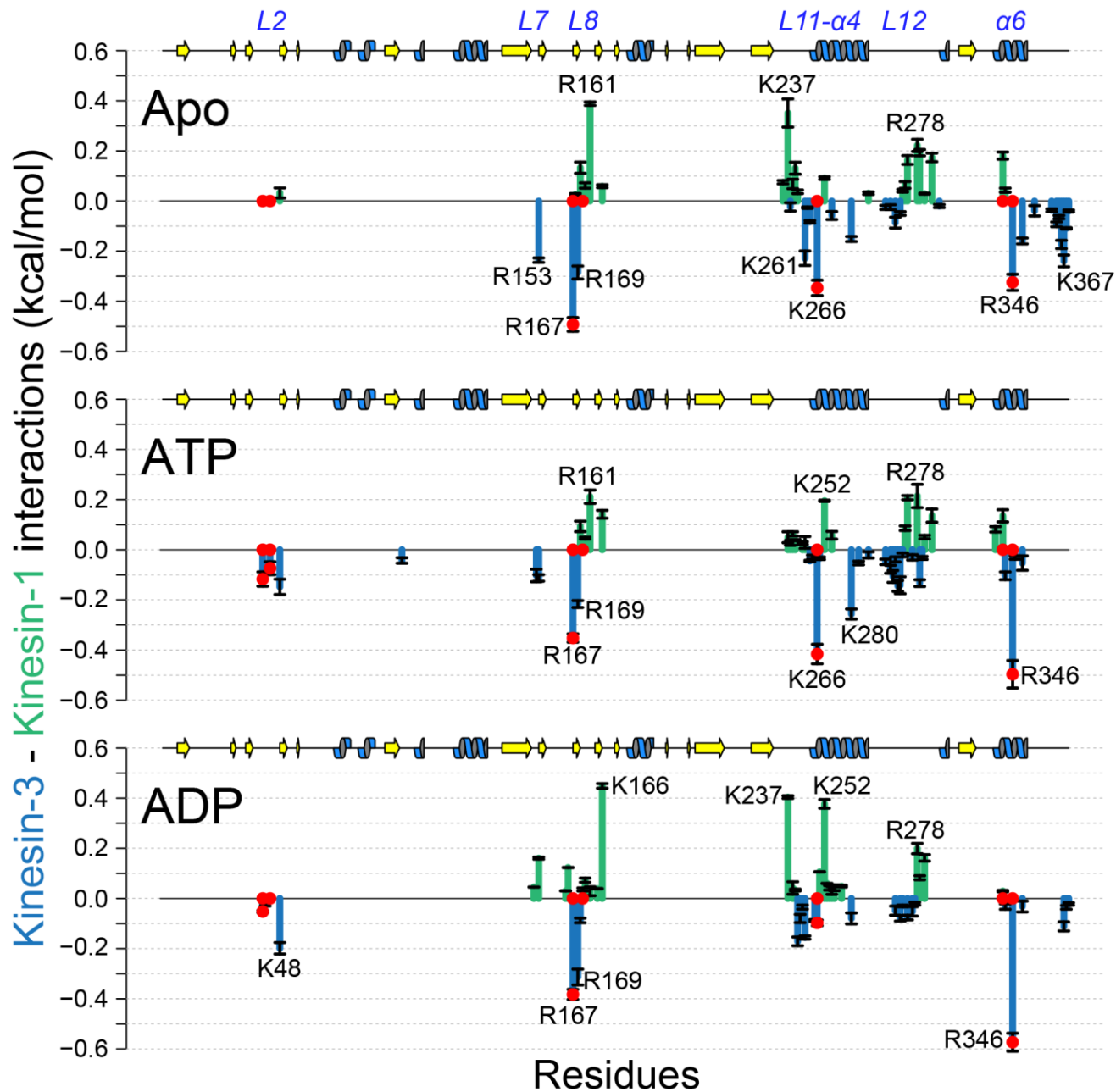


**Figure S5. Differences in residue contribution to binding energy for kinesin-1 (green) and kinesin-3 (blue) in the Apo, ATP and ADP states.** These values were determined from 4 replicate 40ns molecular dynamics simulations and subsequent energetic calculations. The location of residues subjected to mutagenesis simulations and single molecule experiments are indicated with red points.

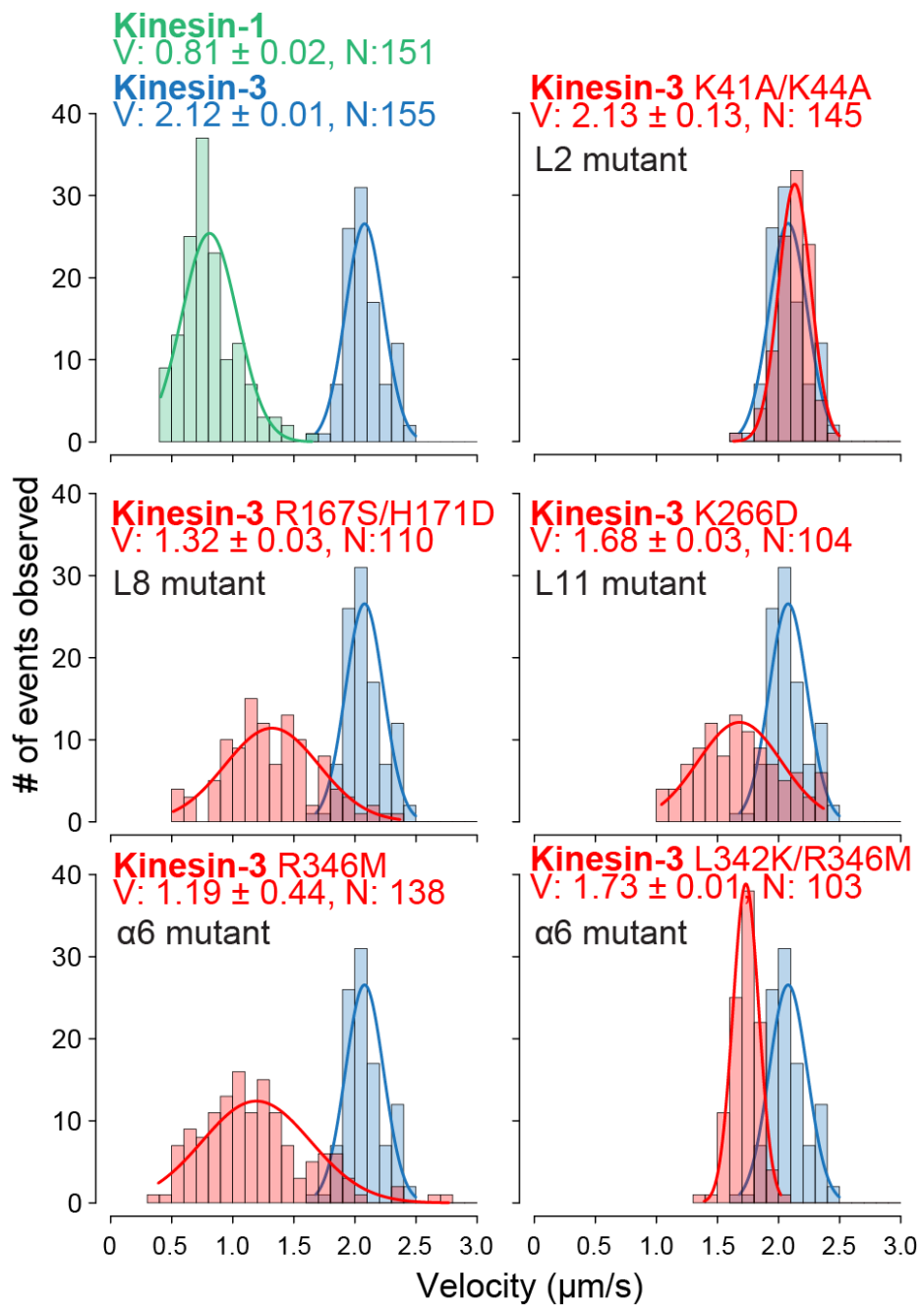
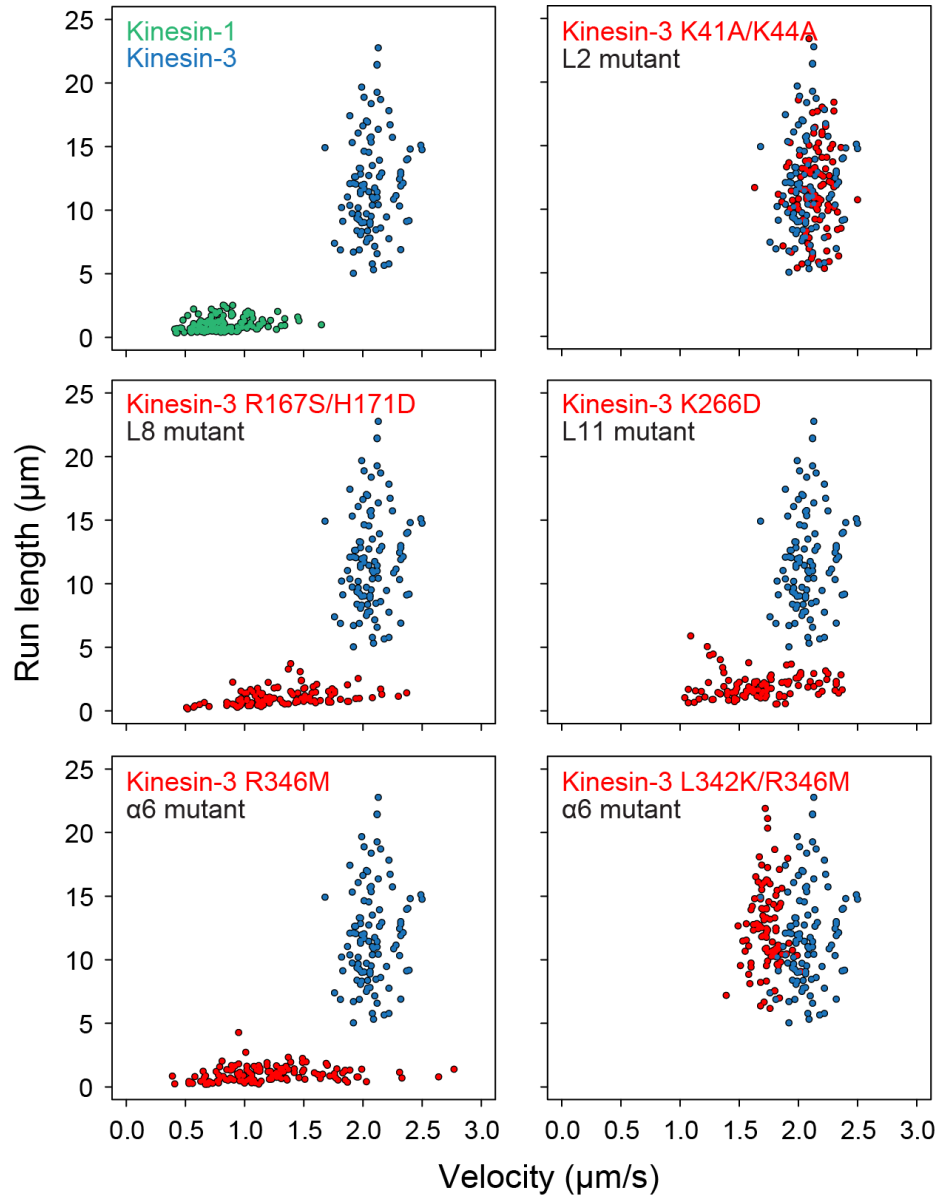
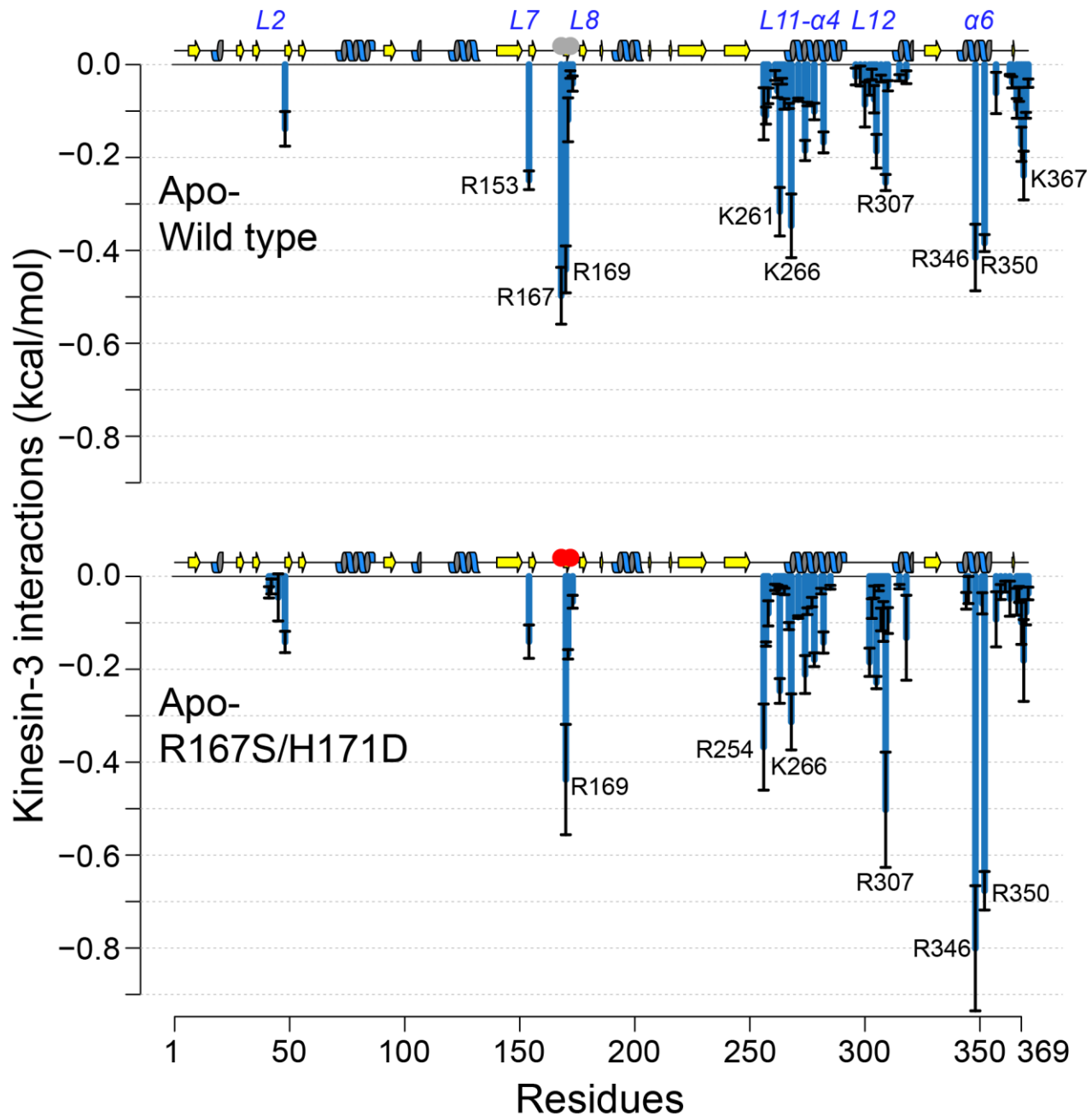


Figure S6. Experimental velocity measurements for kinesin-1 wild type, kinesin-3 wild type and kinesin-3 mutants.



**Figure S7. Experimental velocity versus Run length measurements for kinesin-1 wild type (green), kinesin-3 wild type (blue) and kinesin-3 mutants (red).**



**Figure S8. Results for the kinesin-3 L8 double mutant R167S/H171D in the Apo state.** Kinesin residues with prominent contributions are labeled in black. The mutation sites are indicated with gray points in the WT plot and with red points in the L8 mutant plot. Note the absence of contributions from position 167 in the mutant but enhanced contributions from R307, R346 and R350.